

MultiHuman-Testbench: Benchmarking Image Generation for Multiple Humans

Shubhankar Borse[§] Seokeon Choi Sunghyun Park Jeongho Kim Shreya Kadambi
 Risheek Garrepalli Sungrack Yun Munawar Hayat[§] Fatih Porikli
 Qualcomm AI Research*
[§]{sborse, mhayat}@qti.qualcomm.com

Abstract

Generation of images containing multiple humans, performing complex actions, while preserving their facial identities, is a significant challenge. A major factor contributing to this is the lack of a dedicated benchmark. To address this, we introduce MultiHuman-Testbench, a novel benchmark for rigorously evaluating generative models for multi-human generation. The benchmark comprises 1800 samples, including carefully curated text prompts, describing a range of simple to complex human actions. These prompts are matched with a total of 5,550 unique human face images, sampled uniformly to ensure diversity across age, ethnic background, and gender. Alongside captions, we provide human-selected pose conditioning images which accurately match the prompt. We propose a multi-faceted evaluation suite employing four key metrics to quantify face count, ID similarity, prompt alignment, and action detection. We conduct a thorough evaluation of a diverse set of models, including zero-shot approaches and training-based methods, with and without regional priors. We also propose novel techniques to incorporate image and region isolation using human segmentation and Hungarian matching, significantly improving ID similarity. Our proposed benchmark and key findings provide valuable insights and a standardized tool for advancing research in multi-human image generation. The dataset and evaluation codes will be available at <https://github.com/Qualcomm-AI-research/MultiHuman-Testbench>.

1 Introduction

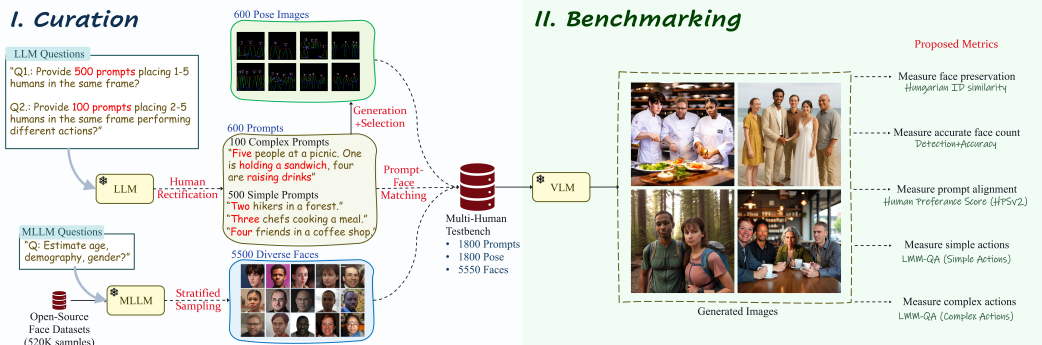


Figure 1: **MultiHuman Testbench**. Our MultiHuman Testbench consists of 5,550 IDs across 1800 samples, including captions describing a scene with of 1-5 humans.

*Qualcomm AI Research is an initiative of Qualcomm Technologies, Inc.

While current text-to-image diffusion models can generate high fidelity images, generating scenes featuring multiple humans (from provided reference images) performing text-described actions still remains a challenge. It requires simultaneously preserving visual characteristics of multiple subjects, accurately rendering their relative positions and interactions, and seamlessly integrating them into the synthesized background. However, current methods [41, 12, 40] frequently exhibit issues such as identity blending, generating the incorrect number of humans, or difficulties in composing the scene according to the text. To make the task easier, some works [19, 6] adopt regional priors as an input to the model, such as human poses, bounding boxes or segmentation masks. While this improves performance, it hinders usability as pose or mask information might not be readily available.

A major challenge in multi-human generation is the lack of a comprehensive and standardized benchmark, along with well defined metrics. Existing benchmarks typically focus on single-subject fidelity [9], general text-to-image quality [4, 46], or multi-object compositional tasks [22, 11]. However, none of the currently available open benchmarks address the added complexity of generating multiple distinct humans. To address this issue, we introduce MultiHuman-Testbench, a novel and challenging benchmark. It is built upon a dataset of 1800 samples, which include carefully crafted text prompts describing scenes with 1 to 5 humans, paired with 5,550 reference human faces, sampled from open-source datasets. We ensure diversity in age, ethnicity, and gender. As many current works rely on regional priors in multi-human scenes [19, 6], we provide pose conditioning images. Additionally, we propose a multi-faceted evaluation framework designed to capture the nuances of multi-human generation. We propose four complementary metrics: Count Accuracy, Hungarian ID similarity, Human Preference Score, Multimodal LLM (MLLM) question-answering to probe the correctness of simple and complex actions. The proposed testbench has four different tasks: 1) Reference-based Multi-Human Generation in the wild. 2) Reference-based Multi-Human Generation with Regional Priors. 3) ID-Consistent Multi-Human Generation without Reference Images. 4) Text-to-Image Multi-Human Generation. We benchmark current models and identify key areas for improvement. Overall, most methods without regional priors struggle in generating the correct number of people. While proprietary models such as GPT-Image-1 generates plausible images, it lacks preserving facial features and has poor ID retention. We also study biases in current models, in terms of gender, age, status, and ethnicity.

Reference-based Multi-Human Generation in the wild, is the most challenging and least restrictive task in our testbench. We propose new techniques (Sec. 3) to adapt current methods for improving their performance this task. Specifically, for unified multi-modal architectures [41, 27], we propose a method to isolate the reference images to impact only a specific region within the latent space. To match each reference image to regions, we propose an implicit Hungarian matching guided by human segmentation. Our method enhances the ability to maintain individual identities, reducing subject leakage and improving ID similarity. We extend our proposed techniques to two models, OmniGen [41] and IR-Diffusion [10], resulting in our proposed MH-OmniGen and MH-IR-Diffusion.

In summary, our contributions are:

- Introduction of a novel, large-scale benchmark for multi-human ID image generation, featuring diverse subjects, text, and pose conditioning.
- A comprehensive evaluation suite designed to assess multi-human generation fidelity, including people count accuracy, ID similarity, text-alignment, and MLLM-based assessment.
- An extensive empirical evaluation and thorough analysis of 30 state-of-the-art zero-shot and training-based generative methods on four different tasks.
- A novel training-free enhancement for existing multi-human generation methods, utilizing regional isolation and matching for improved identity and compositional control.

2 Related Work

Native Text-to-Image models: Multiple diffusion based models have been proposed recently [29, 32, 33, 18, 2]. These models exhibit excellent text-to-image generation ability and can be used as base models for generating multiple humans.

Multi-human Generation with native Text-to-Image models: To generate ID-consistent or subject driven images with text-to-image models, recent works employ auxiliary models such as IP-Adapter [43] or ControlNet [45]. There are also tuning-based approaches which exist such as LoRA [13] or MudI [36] for this purpose. These methods typically fall short on multi-human generation in the wild, without any regional priors.

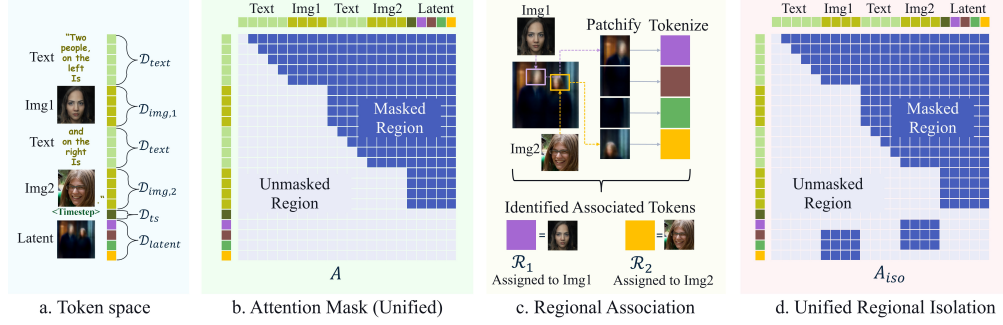


Figure 2: **Regional Isolation for Unified Architectures.** The updates to the attention mask for regional isolation are illustrated in the differences between Fig.b and Fig.d.

ID-Consistent Multi-Human Generation without reference images: Methods such as Consistency [36], DreamStory [11], IR-Diffusion [10] and StoryDiffusion [47] have recently gained popularity in ID-consistent multi-subject generation without reference images. These methods generate human faces and use these faces to generate multiple images for tasks like storytelling.

Multi-Object Generation: Recent approaches e.g., MS-Diffusion [38], MIP-Adapter [14], Lambda-Eclipse [28], have shown significant performance gain for incorporating multiple objects in the same scene. These can include daily items and in some cases, pets such as dogs and cats. However, they struggle to adapt to multi-human generation as zero-shot ID-preservation is a highly challenging task.

Multi-human Generation with native Multi-Modal models: Unified multimodal models, such as OmniGen [41], Show-O [42], OneDiffusion [23] ACE++ [26], GPT-Image-1 [27] and JanusFlow [25] process the text and vision via same transformer backbone and have shown promises for subject-driven generation. These methods input both the reference images and text prompt in a unified token space, removing the need for additional auxiliary task-specific networks such as IP-Adapter/ControlNet. Omnigen [41] was further tuned for ID-preservation. Our evaluations show that among all open-source models, Omnigen produces best results.

Regional Isolation: For networks generating images using simply text inputs, recent works such as IR-Diffusion [10] and InstantFamily [19] have proposed methods such as image isolation and repositional attention, which successfully localize multiple humans in the scene by isolating them from each other and mapping them to separate regions in the image latent. These methods have shown great promise in reducing leakage between multiple human identities.

3 Proposed Approach: Enhancing Existing Methods

Reference-based Multi-human generation in the wild (Task 1 in 5.1) is a highly challenging problem. It requires to preserve input identity while rendering the complete scene with the correct number of humans performing a described action. Using insights from benchmarking current approaches in Section 5, we observe several limitations, including identity blending or missing identities. To tackle these issues, we propose two techniques: **Unified Regional Isolation** and **Implicit Regional Assignment**, that can be flexibly incorporated with existing methods to enhance their quality.

Unified Regional Isolation: Motivated by [19, 10] for T2I architectures, we develop a regional isolation masking strategy to tackle the limitations relating to identity blending and missing, tailored for unified models such as OmniGen [41].

Consider the token space for a unified multimodal model represented in Figure 2 (a). Let L be the total sequence length, and let $i, j \in \{1, \dots, L\}$ be the indices for query and key/value tokens. We define disjoint sets of indices for each token type: $\mathcal{D}_{\text{text}}$, \mathcal{D}_{img} , \mathcal{D}_{ts} (for timestep), and $\mathcal{D}_{\text{latent}}$. Using the setup from OmniGen [41] and Show-o [42], the self-attention mask A ($L \times L$) is constructed based on the type of the query token i : causal attention for text queries, and bidirectional attention for non-text queries (image, timestep, latent). This is represented as:

$$A_{ij} = \begin{cases} 1 & \text{if } i \in \mathcal{D}_{\text{text}} \text{ and } j \leq i \quad (\text{text query: causal}) \\ 1 & \text{if } i \notin \mathcal{D}_{\text{text}} \quad (\text{non-text query: bidirectional}) \\ 0 & \text{otherwise} \end{cases}$$

Consider the tokens in \mathcal{D}_{img} are derived from N distinct original input images, $\{I_1, \dots, I_N\}$. For each image I_k ($k = 1, \dots, N$), let $\mathcal{D}_{\text{img},k} \subseteq \mathcal{D}_{\text{img}}$ be the set of sequence indices corresponding to its derived tokens. These sets partition \mathcal{D}_{img} . This is represented in Figure 2 for $(k = 1, 2)$. For each reference image I_k , consider that we find a region of interest (ROI) set $\mathcal{R}_k \subseteq \mathcal{D}_{\text{latent}}$. Now, we construct a new attention mask \mathbf{A}_{iso} ($L \times L$) such that it isolates the images I_k to only the specific region \mathcal{R}_k within the latent. Hence, our proposed attention mask is computed as:

$$A_{\text{iso},ij} = \begin{cases} 1 & \text{if } i \in \mathcal{D}_{\text{text}} \text{ and } j \leq i \quad (\text{text query: causal}) \\ 1 & \text{if } i \in \mathcal{D}_{\text{img}} \text{ and } (j \notin \mathcal{D}_{\text{latent}} \text{ or } j \in \mathcal{R}_k \text{ where } i \in \mathcal{D}_{\text{img},k}) \quad (\text{image query: ROI attention}) \\ 1 & \text{if } i \in \mathcal{D}_{\text{ts}} \cup \mathcal{D}_{\text{latent}} \quad (\text{timestep/latent query: bidirectional}) \\ 0 & \text{otherwise.} \end{cases}$$

Implicit Region Assignment: To construct the attention mask \mathbf{A}_{iso} , we need region of interest for every image \mathcal{R}_k . This can be done explicitly as in recent methods InstantFamily [19] and Regional Prompting [6], or using a regional prior (pose conditioning or bounding boxes). However, this severely hinders usability, as the users might not want to seek for a multi-human pose image resembling the one which they wish to generate. Hence, to facilitate the generation of multi-human images in the wild, we propose an implicit region assignment strategy that utilize intermediate attention scores and Hungarian matching to assign each reference image to a selected region-of-interest.

Below, we discuss adaptation of our proposed techniques for different models including Omingen [41] and IR-Diffusion [10]. See Appendix C for further details and algorithms.

MH-Omnigen: To find optimal regions for architectures such as Omnigen [41] which have a unified token space for text and reference images, we probe the backbone transformer model at an intermediate timestep. The self-attention maps in the backbone transformer model provide information for the regional overlap for reference images, and the segmentation masks of the intermediate latents provide regional information for each generated person. We perform hungarian matching to find reference inputs with the maximum self-attention region, to eventually find \mathcal{R}_k .

MH-IR-Diffusion: In the case for IR-Diffusion [10], the region-of-interest is defined by the models initially generated images. Similar to the original work, we use a segmentation model, SAM2 [31] to generate the region proposals for generated faces. Next, we compute Arcface similarity between generated faces and reference faces to find the best match, and utilize hungarian matching to assign segments of the matched faces as regions \mathcal{R}_k .

Our experiments in Sec. 5 show that Regional Isolation and Implicit Assignment are training-free plug-and-play methods which can effectively improve different baselines. Due to the implicit matching of identities and localization, we get improved ID similarity with reduced subject blending artifacts.

4 MultiHuman Testbench

Below we elaborate the process of curation of our proposed testbench, and discuss different metrics.

4.1 Image Selection

We curate images using three existing large-scale image datasets, FFHQ [17], SFHQ [1] and CelebA HQ [16], which initially contained approximately 520k samples. These datasets underwent a multi-stage filtering process, where initially we removed human IDs deemed non-"identifiable", using MLLM [24] VQA. We prompt the MLLM with the question "Is the person's face identifiable AND unobstructed?" The images with negative response are filtered out. Subsequently, we identify multi-face images using face detection and eliminate them. These steps reduced the dataset size to 94k distinct human face images. For annotation, we employed Gemini Flash 2.0 to classify each of these images based on three predefined attributes: estimated age-bracket (one of 16-35, 35-60, 60+), estimated demographic (sorted into 6 categories: Caucasian/White, Black/Native African, South-Asian, East-Asian, Hispanic/Latin, Middle

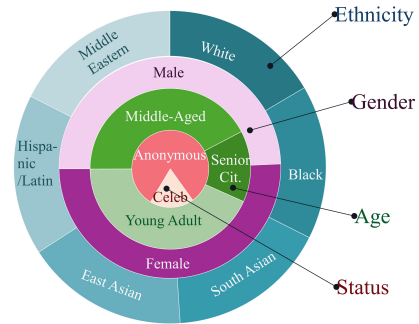


Figure 3: **Data distribution** among four major attributes: Ethnicity, Age, and Gender, Status. See Appendix B for details.

4.5 Metrics

To evaluate multi-human image generation, our benchmark proposes a suite of metrics specifically designed to capture various critical aspects of the generated output.

Hungarian ID Similarity. We propose an ID similarity metric using ArcFace embeddings [8]. To match input and generated IDs in the multi-human setting, we use cosine similarity of Arcface embeddings, and use the hungarian algorithm [21] to match each face while maximizing cost. The Hungarian ID similarity for a given image is thus the average matched ID similarity.

Consider a set of N input face images, indexed by $i = 1, \dots, N$, and a set of M output face detections in the generated image, indexed by $j = 1, \dots, M$. Consider Arcface embeddings for input images $\mathbf{F}^{\text{ref}} = \{\mathbf{f}_i^{\text{ref}} \mid i = 1, \dots, N\}$, where $\mathbf{f}_i^{\text{ref}} \in \mathbb{R}^d$ and for generated faces $\mathbf{F}^{\text{gen}} = \{\mathbf{f}_j^{\text{gen}} \mid j = 1, \dots, M\}$, where $\mathbf{f}_j^{\text{gen}} \in \mathbb{R}^d$. Here, d is the dimensionality of the feature space. Next, we define the similarity s_{ij} between reference face i and generated face j using cosine similarity:

$$s_{ij} = \text{cosSim}(\mathbf{f}_i^{\text{ref}}, \mathbf{f}_j^{\text{gen}}) = \frac{(\mathbf{f}_i^{\text{ref}})^\top \mathbf{f}_j^{\text{gen}}}{\|\mathbf{f}_i^{\text{ref}}\|_2 \|\mathbf{f}_j^{\text{gen}}\|_2}$$

We form an $N \times M$ similarity matrix \mathbf{S} , where $\mathbf{S}_{ij} = s_{ij}$. Since the Hungarian algorithm finds a minimum cost assignment, we define the cost c_{ij} as the negative similarity, $c_{ij} = -s_{ij}$. Using the Hungarian algorithm, we find a binary assignment matrix \mathbf{X} ($X_{ij} = 1$ if matched, 0 otherwise). For each reference input i , if reference i is matched to a generated face j (i.e., $\sum_{k=1}^M X_{ik} = 1$), its contribution to the ID metric is the similarity s_{ij}/N for the matched j . If reference i is not matched to any generated face (i.e., $\sum_{k=1}^M X_{ik} = 0$), its contribution to the ID metric is 0. Hence, the average similarity over all N reference inputs, denoted S_{id} , is denoted as: $S_{id} = \frac{1}{N} \sum_{i=1}^N \sum_{j=1}^M X_{ij} s_{ij}$. Our proposed Hungarian ID similarity metric objectively evaluates the model’s effectiveness in maintaining consistent and uniquely recognizable identities across different generations. Further, the proposed metric penalizes for subject/ID mixing.

Count Accuracy. Next, we assess the accuracy of the generated people count. This verifies the model’s ability to precisely adhere to the numerical specification in the prompt. We use a face detection model [7] to count detected human faces in the generated image. Hence, as N is the number of reference images and M is the number of generated faces, the count accuracy is $S_{\text{count}} = \delta_{MN}$, where δ is the kronecker delta [3] function.

Quality/Prompt Alignment. Third, text alignment for overall scene consistency is evaluated using the HPSv2 score [39], S_{hps} . This metric goes beyond individual elements to measure how well the entire generated image corresponds to the textual description of the scene, ensuring that contexts, environments, and overall narrative specified in the prompt are accurately reflected.

MLLM Action QA. Fourth, to probe the correctness of simple and complex actions and interactions among multiple individuals, we utilize Multimodal Large Language Model (MLLM) question-answering. This approach allows for a deeper semantic evaluation by querying the MLLM about specific details, activities, and relationships depicted in the generated image, thereby assessing challenging compositional aspects. We propose to report the average separately for simple actions (Action-S) and complex actions (Action-C), as they provide deeper meaning. To generate the questions, we probe Gemini-Flash to extract actions from each text prompt, and re-contextualize these into questions. For instance, assume the prompt is "Five people caroling during winter: among them, two people are holding song books, and three people are singing". For this prompt, the questions which are generated to rank complex actions are as follows: "Q1: Are two people in this image holding song books? Choices: 1(No), 10(Yes), 5(Partially)? Q2: Are the people in this image caroling? Choices: 1(No), 10(Yes), 5(Partially)?". Hence, the final (Action-C) score is the average score.

5 Benchmarking

We benchmark models under four settings: 1). Reference-based Multi-Human Generation in the wild, 2). Reference-based Multi-Human Generation with Regional Priors, 3). Story Consistent Multi-Human generation without reference images and 4). Text-to-Image multi-human generation without reference images. We use tuning-based methods such as LoRA [13] and MuDI [15] on SDXL [29]. For each prompt, we tune a single LoRA for all concepts, using the method in [15]. Next, we benchmark methods trained for general multi-subject generation, MS-Diffusion [38], MIP-

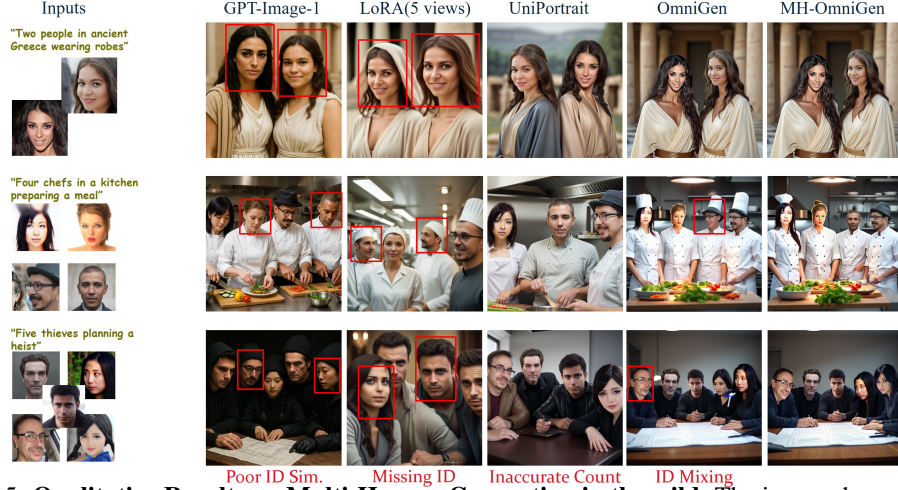


Figure 5: **Qualitative Results on Multi-Human Generation in the wild.** The image shows the best performing methods: UniPortrait, LoRA, GPT-Image-1, OmniGen and MH-OmniGen.

Adpater [14] and Lambda-Eclipse [28]. For multi-human generation, we evaluate UniPortrait [12], RectifID [35], Fastcomposer [40], OmniGen [41] and GPT-Image-1 [27]. We also benchmark methods which require explicit regional priors such as Regional-Prompting [6] with PuLID [9], and OMG [20] with InstantID [37]. Furthermore, we evaluate story-based(reference-free) diffusion models, Consistory [36], DreamStory [11] and IR-Diffusion [44] on our proposed benchmark. Finally, we evaluate native text-to-image models, SD-1.5 [32], RV-1.5 [33], SDXL [29], SD3.5 [2], FLux [18] and OmniGen [41], for generating accurate number of humans. All implementation details and hyperparameters are provided in Appendix D.

5.1 Results

Task 1. Reference-based Multi-Human Generation in the Wild:

Our results for task 1 are summarized in Table 1. We evaluate the performance of four different types of models: Proprietary, Tuning-based, Multi-Object Tuning-Free and Multi-Human Tuning-Free methods. From the scores, we find that the performance of each method is significantly influenced by the backbone model it builds upon. On average, **Multi-object Tuning-Free methods** perform worse compared to other approaches. This is because generating humans and keeping their likeness intact is a significantly challenging problem, compared to the objects the methods have been trained on. Next, **Tuning-based methods** MuDI [15] and LoRA [13] perform slightly better, but are significantly bounded by the base architecture SDXL. As observed, training with 5 views generated from PuLID [9] performs better than a single view. Moving to **Multi-Human Tuning-free** approaches, we can observe that UniPortrait [12], built on RV1.5, significantly outperforms other SD1.5-based approaches such as RectifID [35] and FastComposer [40] across all metrics. However, unified multi-modal models, OmniGen [41] and GPT-Image-1 [27], perform significantly better than the rest. Notably, our proposed MH-OmniGen consistently outperforms its predecessor across four of the five metrics. We observe a **5.1** point difference in Multi-ID and **4.1** point difference in action similarity. This validates the effectiveness of our Unified Regional Isolation and Implicit Assignment method. Finally, among all evaluated methods, GPT-4o (via GPT-Image-1) achieves the highest overall performance in count accuracy, HPS, and action-based metrics. However, its performance in ID similarity is notably weaker (**25.7** points) than MH-OmniGen. This is due to the fact that GPT hallucinates features on humans, and in many cases isn't able to effectively maintain the identity of the person. **Overall**, we want to stress that **None** of the methods perform consistently well at a high standard for this task in terms of visual quality. Within the open-source methods, **None** of the models can consistently generate images with a high Action-C or Count score. There is significant scope for improvement in this setting.

Qualitative Results: In Figure 5, we show visual Results for the best models performing Task 1. As observed in this image, GPT-1 isn't able to effectively maintain human ID, owing to poor scores. On the other hand, Uniportrait generates good results but often with the inaccurate number of

humans. OmniGen results have artifacts related to ID mixing, which are considerably repaired in MH-OmniGen. However, OmniGen-based methods tend to "copy" human faces. It is important to note that these are some of the better looking images for each method. We share more visual results in the Appendix, highlighting a heavy scope for improvement.

	Backbone	Model	Count	Multi-ID	HPS	Action-S	Action-C
Task 1: Reference-based Multi-Human Generation in the Wild							
Proprietary	GPT-4o	GPT-Image-1	87.9	28.8	30.3	97.0	91.1
Tuning-Based	SDXL	LoRA(1 view)	47.3	20.2	25.3	61.0	55.4
		LoRA(5 views)	52.6	22.0	25.9	73.0	72.9
		MuDI(1 view)	48.1	23.6	24.8	64.0	51.5
		MuDI(5 views)	53.9	24.6	25.6	67.3	71.5
Multi-Object Tuning-Free	SDXL	IP-Adapter	34.3	9.3	23.2	49.6	46.9
		MIP-Adapter	39.2	11.9	24.0	57.6	53.7
	Kand2.2	Lamda-Eclipse	53.3	12.5	23.4	56.1	50.8
Multi-Human Tuning-Free	RV1.5	UniPortrait	58.5	44.2	25.9	76.2	67.2
	SD1.5	RectifID	37.8	18.6	24.8	67.3	68.2
		Fastcomposer	31.2	12.2	21.7	48.9	41.2
	Phi-3	OmniGen	60.5	49.4	26.2	87.5	71.3
		MH-Omnigen	60.3	54.5	26.3	91.6	72.9

Table 1: Multi-Human Generation with Reference Images in the wild.

Task 2. Reference-based Multi-Human Generation with Regional Priors:

Next, we evaluate methods for Task 2, which focuses on reference-based multi-human generation with regional priors. Table 2 shows results for Tuning-based, Multi-Object Tuning-Free, and Multi-Human Tuning-Free methods, all leveraging pose or box priors. As observed, the introduction of our provided human-rectified pose priors significantly improves quantitative metrics, particularly Count accuracy, compared to Task 1. We also observe a general increase in Action scores. For instance, MIP-Adapter [14] shows significantly higher Count accuracy with pose priors. Within the Multi-Human Tuning-Free group, we observe varied performance across metrics depending on the backbone and specific prior usage. RectifID [35] achieves the highest Count accuracy (**90.1**), while OMG-InstantID [20] (SDXL) excels in HPS (**27.2**) and Action scores (**90.4**, **78.9**), and Regional-PuLID [6] (Flux) shows the strongest Multi-ID retention (**50.7**). OmniGen demonstrates competitive performance in Task 2, maintaining strong HPS (**27.4**) and Action scores (**86.2**) and decent Multi-ID (**48.2**) when incorporating pose priors. Overall, Task 2 results highlight the significant benefit of regional guidance for key metrics like count, while demonstrating that achieving high performance across all aspects (like ID fidelity, action, and overall quality) remains a challenge. This is due to the fact that different methods are strong in different areas.

	Backbone	Model	Regional Conditioning	Count	Multi-ID	HPS	Action-S	Action-C
Task 2: Reference-based Multi-Human Generation with Regional Priors								
Tuning-based	SDXL	LoRA(1 view)	Pose	85.3	17.3	26.1	73.6	78.0
		LoRA(5 views)		<u>89.6</u>	21.4	26.0	77.7	73.6
Multi-Object Tuning-Free	SDXL	MIP-Adapter	Pose	81.5	14.1	25.0	69.2	67.2
Multi-Human Tuning-Free	Flux	Regional-PuLID	Boxes	67.4	50.7	26.1	74.1	68.0
	Flux	Flux-Kontext	Boxes	76.8	39.2	26.9	80.9	79.8
	RV1.5	UniPortrait	Pose	78.3	49.2	26.3	<u>88.2</u>	<u>78.1</u>
	SD1.5	RectifID	Pose	90.1	26.4	25.7	78.7	73.5
	SDXL	OMG-InstantID	Pose	71.2	32.6	<u>27.2</u>	90.4	78.9
	Phi-3	OmniGen	Pose	77.2	48.2	27.4	86.2	75.3

Table 2: Multi-Human Generation with Reference Images, with regional priors

Task 3. ID-Consistent Multi Human Generation without reference images:

Table 3 displays results on Task 3. We benchmarked four approaches. The performance varies across metrics, with ConsiStory and DreamStory showing lower accuracy in Count and ID-Similarity compared to IR-Diffusion and MH-IR-Diffusion. Notably, MH-IR-Diffusion achieved the highest scores in both Count (**62.6**) and Multi-ID (**33.3**). Due to the process of masking and hungarian assignment, the model is successfully able to preserve ID information while keeping the remaining

metrics stable. While IR-Diffusion led slightly in Action-S (**86.3**), and all models performed similarly on HPS. We observe for the Complex Action metrics, that the performance reduces slightly as ID similarity improves. This is due to the fact that the results are closer to original model generation, as lesser ID’s have been matched. Overall, we see a significant scope of improvement for every method in this list, due to poor performance on all metrics.

Backbone	Model	Resolution	Metrics				
			Count	Multi-ID	HPS	Action-S	Action-C
Task 3: ID-Consistent Multi-Human Generation without Reference Images							
Playground-v2.5	ConsiStory	768 × 1280	44.6	16.2	28.0	84.1	71.9
	DreamStory		45.0	19.7	28.2	84.8	71.8
	IR-Diffusion		62.4	<u>27.6</u>	<u>29.4</u>	86.3	<u>71.8</u>
	MH-IR-Diffusion		62.6	33.3	29.2	<u>85.9</u>	71.3

Table 3: Multi-Human Generation without Reference Images

Task 4. Text-to-image Multi-Human Generation:

For Task 4, we evaluate the overall effectiveness of text-to-image methods on generating humans with accurate count performing text-described simple and complex action. This is mainly to motivate the selection of a suitable base architecture for follow-up methods to build their solutions on. Our results are summarized in Table 4. Across all methods we evaluated, Flux, SD3.5 and OmniGen perform best, given the fact that they are larger models and have been trained on richer data. Notably, Flux produces images with consistent Count accuracy over 3, 4, 5 humans, compared to the other methods which show a steeper drop in performance after increasing the number of humans. SD3.5 is highly competitive in generating the correct actions (simple and complex), and OmniGen produces the best HPS. Overall, however, there is significant scope for improvement in terms of human count, as the best score (**63.9**) is still quite low.

Model	Person Count				Prompt Alignment		
	3-Person	4-Person	5-Person	Avg(1-5)	HPS	Action-S	Action-C
Task 4: Text-to-Image Multi-Human Generation							
SD-1.5	25.0	12.8	7.4	26.6	24.8	84.5	73.3
RV-1.5	52.5	20.3	11.5	43.5	26.9	88.3	76.0
SDXL	44.0	30.7	23.5	43.3	26.9	87.9	79.1
SD3.5	61.0	<u>45.6</u>	28.8	<u>56.1</u>	27.8	95.7	85.0
OmniGen	<u>64.0</u>	29.0	<u>33.2</u>	53.8	28.7	93.2	82.5
Flux-Dev	66.9	57.0	46.4	63.9	<u>28.2</u>	92.6	83.0

Table 4: Benchmarking Foundational Text-to-Image models on generating multiple people.

5.2 Scope for Improvement

From the analysis in this Section and in Appendix E,F, we uncover several limitations of current approaches performing Multi-Human Generation. **First**, we notice that without regional priors, the open-source models performing Tasks 1, 2, 4 are lacking in terms of the person count and complex actions. Essentially, this means that multi-human generation is significantly hindered because the base model itself (from task 4) isn’t able to generate an accurate number of human faces in a scene within the text described action. **Second**, we notice that none of the methods (with OR without regional priors) consistently pass the eye test in generating images of the correct number of people while maintaining a high ID similarity, and sufficient action scores. This balance is essential for our proposed task, and remains an open challenge. **Third**, in Appendix E, we observe that several methods contain implicit biases over age, racial profile and gender. After uncovering these biases, we hope that the community strives to reduce them using insights from our benchmark.

6 Conclusion

This paper introduces MultiHuman-Testbench, the first large-scale benchmark for Subject-Driven Image Generation with Multiple Identities. Complementing the benchmark, we provide a multi-faceted suite of metrics designed to capture various aspects of generation quality. We also propose enhancements to current methods for multi-human generation to improve their performance. Finally, we benchmark approximately 30 models across four distinct tasks, analyzing their performance and outlining the scope for future improvement. We believe the analysis will greatly benefit the

community and facilitate collaborative efforts to address the challenging problem of Multi-Human generation.

References

- [1] Rameen Abdal, Peihao Zhu, Niloy Mitra, and Peter Wonka. Styleflow: Attribute-conditioned exploration of stylegan’s latent space. *ACM Transactions on Graphics (TOG)*, 39(6):1–17, 2020.
- [2] Stability AI et al. Stable diffusion 3. *arXiv preprint arXiv:2403.03204*, 2024.
- [3] George Arfken. *Mathematical Methods for Physicists*. Academic Press, Inc., San Diego, third edition, 1985.
- [4] Yujie Bai, Karthik Kadavath, Tamera Askell, Andy Chen, Anna Jones, Scott McKinnon, Sam Olsson, Josh Henighan, Dario Perez, Nicholas Wu, et al. Aligning text-to-image models using human preferences. *arXiv preprint arXiv:2305.18290*, 2023.
- [5] Clément Bonnet, Ariel N Lee, Franck Wertel, Antoine Tamano, Tanguy Cizain, and Pablo Ducru. From text to pose to image: Improving diffusion model control and quality. *arXiv preprint arXiv:2411.12872*, 2024.
- [6] Anthony Chen, Jianjin Xu, Wenzhao Zheng, Gaole Dai, Yida Wang, Renrui Zhang, Haofan Wang, and Shanghang Zhang. Training-free regional prompting for diffusion transformers. *arXiv preprint arXiv:2411.02395*, 2024.
- [7] Jiankang Deng, Jia Guo, Evangelos Ververas, Irene Kotsia, and Stefanos Zafeiriou. Retinaface: Single-shot multi-level face localisation in the wild. In *Proceedings of the IEEE/CVF Conference on Computer Vision and Pattern Recognition*, pages 5203–5212, 2020.
- [8] Jiankang Deng, Jia Guo, Niannan Xue, and Stefanos Zafeiriou. Arcface: Additive angular margin loss for deep face recognition. In *Proceedings of the IEEE/CVF conference on computer vision and pattern recognition*, pages 4690–4699, 2019.
- [9] Zinan Guo, Yanze Wu, Chen Zhuowei, Peng Zhang, Qian He, et al. Pulid: Pure and lightning id customization via contrastive alignment. *Advances in neural information processing systems*, 37:36777–36804, 2024.
- [10] Huiguo He, Qiuyue Wang, Yuan Zhou, Yuxuan Cai, Hongyang Chao, Jian Yin, and Huan Yang. Improving multi-subject consistency in open-domain image generation with isolation and reposition attention. *arXiv preprint arXiv:2411.19261*, 2024.
- [11] Huiguo He, Huan Yang, Zixi Tuo, Yuan Zhou, Qiuyue Wang, Yuhang Zhang, Zeyu Liu, Wenhao Huang, Hongyang Chao, and Jian Yin. Dreamstory: Open-domain story visualization by llm-guided multi-subject consistent diffusion. *arXiv preprint arXiv:2407.12899*, 2024.
- [12] Junjie He, Yifeng Geng, and Liefeng Bo. Uniportrait: A unified framework for identity-preserving single-and multi-human image personalization. *arXiv preprint arXiv:2408.05939*, 2024.
- [13] Edward J Hu, Yelong Shen, Phillip Wallis, Zeyuan Allen-Zhu, Yanzhi Li, Shean Wang, Lu Wang, Weizhu Chen, et al. Lora: Low-rank adaptation of large language models. *ICLR*, 1(2):3, 2022.
- [14] Qihan Huang, Siming Fu, Jinlong Liu, Hao Jiang, Yipeng Yu, and Jie Song. Resolving multi-condition confusion for finetuning-free personalized image generation. In *Proceedings of the AAAI Conference on Artificial Intelligence*, volume 39, pages 3707–3714, 2025.
- [15] Sangwon Jang, Jaehyeong Jo, Kimin Lee, and Sung Ju Hwang. Identity decoupling for multi-subject personalization of text-to-image models. *arXiv preprint arXiv:2404.04243*, 2024.
- [16] Tero Karras, Timo Aittala, and Samuli Laine. Progressive growing of gans for improved quality, stability, and variation. In *International Conference on Learning Representations (ICLR)*, 2018.

- [17] Tero Karras, Samuli Laine, Timo Aittala, Janne Hellsten, Jaakko Lehtinen, and Timo Knuuttila. A style-based generator architecture for generative adversarial networks. In *Proceedings of the IEEE/CVF Conference on Computer Vision and Pattern Recognition (CVPR)*, pages 4401–4410, 2019.
- [18] Sherif Khalifa, Steven Shleifer, Alex Timofeev, Xuyang Wang, Yu Che, Hyunwoo Lee, Weiyue Li, Xin Tang, Aleksandra Mojsilovic, Ashish Shrivastava, et al. Diffusion models for vision-language modeling. *arXiv preprint arXiv:2403.08558*, 2024.
- [19] Chanran Kim, Jeongin Lee, Shichang Joung, Bongmo Kim, and Yeul-Min Baek. Instantfamily: Masked attention for zero-shot multi-id image generation. *arXiv preprint arXiv:2404.19427*, 2024.
- [20] Zhe Kong, Yong Zhang, Tianyu Yang, Tao Wang, Kaihao Zhang, Bizhu Wu, Guanying Chen, Wei Liu, and Wenhan Luo. Omg: Occlusion-friendly personalized multi-concept generation in diffusion models. In *European Conference on Computer Vision*, pages 253–270. Springer, 2024.
- [21] Harold W. Kuhn. The hungarian method for the assignment problem. *Naval Research Logistics Quarterly*, 2(1-2):83–97, 1955.
- [22] Nupur Kumari, Bingliang Zhang, Richard Zhang, Eli Shechtman, and Jun-Yan Zhu. Multi-concept customization of text-to-image diffusion. In *Proceedings of the IEEE/CVF conference on computer vision and pattern recognition*, pages 1931–1941, 2023.
- [23] Duong H Le, Tuan Pham, Sangho Lee, Christopher Clark, Aniruddha Kembhavi, Stephan Mandt, Ranjay Krishna, and Jiasen Lu. One diffusion to generate them all. *arXiv preprint arXiv:2411.16318*, 2024.
- [24] Bo Li, Yuanhan Zhang, Dong Guo, Renrui Zhang, Feng Li, Hao Zhang, Kaichen Zhang, Peiyuan Zhang, Yanwei Li, Ziwei Liu, et al. Llava-onevision: Easy visual task transfer. *arXiv preprint arXiv:2408.03326*, 2024.
- [25] Yiyang Ma, Xingchao Liu, Xiaokang Chen, Wen Liu, Chengyue Wu, Zhiyu Wu, Zizheng Pan, Zhenda Xie, Haowei Zhang, Liang Zhao, et al. Janusflow: Harmonizing autoregression and rectified flow for unified multimodal understanding and generation. *arXiv preprint arXiv:2411.07975*, 2024.
- [26] Chaojie Mao, Jingfeng Zhang, Yulin Pan, Zeyinzi Jiang, Zhen Han, Yu Liu, and Jingren Zhou. Ace++: Instruction-based image creation and editing via context-aware content filling. *arXiv preprint arXiv:2501.02487*, 2025.
- [27] OpenAI. Gpt-image-1. <https://platform.openai.com/docs/guides/image-generation?image-generation-model=gpt-image-1>, 2025.
- [28] Maitreya Patel, Sangmin Jung, Chitta Baral, and Yezhou Yang. Lambda-eclipse: Multi-concept personalized text-to-image diffusion models by leveraging clip latent space. *arXiv preprint arXiv:2402.05195*, 2024.
- [29] Dustin Podell, Zion English, Kyle Lacey, Andreas Blattmann, Tim Dockhorn, Jonas Müller, Joe Penna, and Robin Rombach. Sdxl: Improving latent diffusion models for high-resolution image synthesis. *arXiv preprint arXiv:2307.01952*, 2023.
- [30] PopulationPyramid.net. World population pyramid 2024, 2024.
- [31] Nikhila Ravi, Valentin Gabeur, Yuan-Ting Hu, Ronghang Hu, Chaitanya Ryali, Tengyu Ma, Haitham Khedr, Roman Rädle, Chloe Rolland, Laura Gustafson, et al. Sam 2: Segment anything in images and videos. *arXiv preprint arXiv:2408.00714*, 2024.
- [32] Robin Rombach, Andreas Blattmann, Dominik Lorenz, Patrick Esser, and Björn Ommer. High-resolution image synthesis with latent diffusion models. In *Proceedings of the IEEE/CVF Conference on Computer Vision and Pattern Recognition (CVPR)*, pages 10684–10695, 2022.
- [33] SG_161222. Realistic vision v1.3 (and other versions), 2023.

- [34] Arseniy Shakhmatov, Anton Razzhigaev, Aleksandr Nikolich, Vladimir Arkhipkin, vIgor Pavlov, Andrey Kuznetsov, and Denis Dimitrov. kandinsky 2.2, 2023.
- [35] Zhicheng Sun, Zhenhao Yang, Yang Jin, Haozhe Chi, Kun Xu, Liwei Chen, Hao Jiang, Yang Song, Kun Gai, and Yadong Mu. Rectifid: Personalizing rectified flow with anchored classifier guidance. *Advances in Neural Information Processing Systems*, 37:96993–97026, 2024.
- [36] Yoad Tewel, Omri Kaduri, Rinon Gal, Yoni Kasten, Lior Wolf, Gal Chechik, and Yuval Atzmon. Training-free consistent text-to-image generation. *ACM Transactions on Graphics (TOG)*, 43(4):1–18, 2024.
- [37] Qixun Wang, Xu Bai, Haofan Wang, Zekui Qin, Anthony Chen, Huaxia Li, Xu Tang, and Yao Hu. Instantid: Zero-shot identity-preserving generation in seconds. *arXiv preprint arXiv:2401.07519*, 2024.
- [38] Xierui Wang, Siming Fu, Qihan Huang, Wanggui He, and Hao Jiang. Ms-diffusion: Multi-subject zero-shot image personalization with layout guidance. *arXiv preprint arXiv:2406.07209*, 2024.
- [39] Xiaoshi Wu, Yiming Hao, Keqiang Sun, Yixiong Chen, Feng Zhu, Rui Zhao, and Hongsheng Li. Human preference score v2: A solid benchmark for evaluating human preferences of text-to-image synthesis. *arXiv preprint arXiv:2306.09341*, 2023.
- [40] Guangxuan Xiao, Tianwei Yin, William T Freeman, Frédo Durand, and Song Han. Fastcomposer: Tuning-free multi-subject image generation with localized attention. *International Journal of Computer Vision*, pages 1–20, 2024.
- [41] Shitao Xiao, Yuez Wang, Junjie Zhou, Huaying Yuan, Xingrun Xing, Ruiran Yan, Shuting Wang, Tiejun Huang, and Zheng Liu. Omnigen: Unified image generation. *arXiv preprint arXiv:2409.11340*, 2024.
- [42] Jinheng Xie, Weijia Mao, Zechen Bai, David Junhao Zhang, Weihao Wang, Kevin Qinghong Lin, Yuchao Gu, Zhijie Chen, Zhenheng Yang, and Mike Zheng Shou. Show-o: One single transformer to unify multimodal understanding and generation. In *The Thirteenth International Conference on Learning Representations*, 2025.
- [43] Hu Ye, Jun Zhang, Sibio Liu, Xiao Han, and Wei Yang. Ip-adapter: Text compatible image prompt adapter for text-to-image diffusion models. *arXiv preprint arXiv:2308.06721*, 2023.
- [44] Xizhuo Yu, Chaojie Fan, Zhizhong Zhang, Yongbo Wang, Chunyang Chen, Tianjian Yu, and Yong Peng. Identity-aware infrared person image generation and re-identification via controllable diffusion model. *Pattern Recognition*, 165:111561, 2025.
- [45] Shihao Zhao, Dongdong Chen, Yen-Chun Chen, Jianmin Bao, Shaozhe Hao, Lu Yuan, and Kwan-Yee K Wong. Uni-controlnet: All-in-one control to text-to-image diffusion models. *Advances in Neural Information Processing Systems*, 36:11127–11150, 2023.
- [46] Ji Zhou, Kai Yu, Yuanhan Sun, Jianlong Fu, Jinhui Wu, and Tat-Seng Chua. Geneval: A benchmark for evaluating text-to-image generation. *arXiv preprint arXiv:2403.10672*, 2024.
- [47] Yupeng Zhou, Daquan Zhou, Ming-Ming Cheng, Jiashi Feng, and Qibin Hou. Storydiffusion: Consistent self-attention for long-range image and video generation. *Advances in Neural Information Processing Systems*, 37:110315–110340, 2024.

Appendices

A Contents

This appendix provides supplementary material to accompany the main paper. It includes a detailed breakdown of the data distribution used, further specifics on our proposed methodology, implementation details for baselines and our approach, extended quantitative and qualitative results including ablation studies and failure cases, and a discussion on the societal impact of our work. The following sections detail these aspects:

Section A: Contents

Section B: Data Distribution

Section C: Additional Details on Proposed Approach

Subsection C.1: Implicit Region Assignment

Section D: Baselines and Implementation Details

Section E: Additional Quantitative Results

Subsection E.1: Performance across varying number of people

Subsection E.2: Measuring Bias in Multi-Human Generation

Subsection E.3: Effect of Our Pose Priors

Section F: Additional Qualitative Results

Subsection F.1: Improvements from MH-OmniGen

Subsection F.2: Qualitative results for Task 2: Regional Priors

Subsection F.3: Qualitative results for Task 4: Text-to-Image generation

Section G: Societal Impact

B Data Distribution

In this Section, we provide a detailed description of the sampled faces. This is supplementing Figure 3 in the main text.

Attribute	Category	Percentage (%)
Age	Young Adult (16-35)	43.17
	Middle Age (36-60)	42.72
	Aged (60+)	14.11
Gender	Male	49.24
	Female	50.76
Status	Anonymous	81.48
	Celebrity	18.52
Data	Real	72.41
	Synthetic	27.59
Ethnicity	White	16.52
	Black	15.75
	South Asian	16.65
	East Asian	16.72
	Hispanic/Latin	16.74
	Middle Eastern/Other European	17.64

Table B.1: Data Distribution by Attribute. All the labels are obtained by Gemini-Flash-2.0.

C Additional Details on Proposed Approach

In this Section, we provide detailed explanation of our proposed Implicit Region Assignment strategy behind the MH-Omnigen and MH-IR-Diffusion methods. This is an extension of Section 3.

C.1 Implicit Region Assignment

To construct the attention mask \mathbf{A}_{iso} described in Section 3, we need a region of interest (ROI) set $\mathcal{R}_k \subseteq \mathcal{D}_{\text{latent}}$ for every reference image I_k . To facilitate the generation of multi-human images in the wild, we propose an implicit region assignment strategy that utilizes intermediate attention scores and Hungarian matching to assign each reference image to a selected region-of-interest.

MH-Omnigen: For unified architectures, we propose a two-stage process to determine ROIs implicitly from the model’s own understanding and the intermediate latent representation $\mathbf{O}_{\text{int},t}$. This process involves first identifying areas in the latent space which have a high self-attention overlap with each reference image. Next, we segment the estimated image from an intermediate timestep in and assign these segments to the reference images using hungarian matching.

Algorithm 1 Find attention-based similarity maps for Reference Images

Inputs:

- Unified Multimodal Diffusion Model U .
- Intermediate latent $\mathbf{O}_{\text{int},t} \in \mathbb{R}^{D \times D}$ at timestep t .
- Set of K input reference images: $\{I_1, \dots, I_K\}$.
- Image token index sets: $\mathcal{D}_{\text{img},k} \subseteq \{1, \dots, L\}$ for $k = 1, \dots, K$.
- Latent token index set: $\mathcal{D}_{\text{latent}} \subseteq \{1, \dots, L\}$.
- Reshape map $\mathcal{M}_{\text{reshape}} : \mathbb{R}^{|\mathcal{D}_{\text{latent}}|} \rightarrow \mathbb{R}^{D \times D}$, where $|\mathcal{D}_{\text{latent}}| = D \times D$.
- Set of H layers to probe: $\mathcal{L} = \{l_1, \dots, l_H\}$.

Outputs:

- Set of K similarity maps for every reference image: $\{\mathbf{S}_k \mid k = 1, \dots, K\}$, each $\mathbf{S}_k \in \mathbb{R}^{D \times D}$.
-

```

1:                                     ▷ Initialize similarity maps
2: for  $k = 1, \dots, K$  do
3:   Initialize  $\mathbf{S}_k$  as a  $D \times D$  zero matrix.
4:    $\mathbf{S}_k[p, q] = 0$  for all  $(p, q)$ .
5: end for
6:
7:                                     ▷ Iterate through layers
8: for  $l$  in  $\mathcal{L}$  do
9:                                     ▷ Get attention map for layer  $l$  at timestep  $t$ 
10:  Let  $\mathbf{P}^{(l)} \in \mathbb{R}^{L \times L}$  be the self-attention map from layer  $l$ .
11:   $\mathbf{P}_{ij}^{(l)}$  is attention from query token  $i$  to key/value token  $j$ , for  $i, j \in \{1, \dots, L\}$ .
12:                                     ▷ Iterate through all reference images  $I_k$ 
13:  for  $k = 1, \dots, K$  do
14:    ▷ Slice attention maps for latent and aggregate over tokens corresponding to  $I_k$ 
15:    Define flat vector  $\mathbf{V}_{k,l} \in \mathbb{R}^{|\mathcal{D}_{\text{latent}}|}$ .
16:    For each  $i \in \mathcal{D}_{\text{latent}}$ ,  $\mathbf{V}_{k,l}[i] = \sum_{j \in \mathcal{D}_{\text{img},k}} \mathbf{P}_{ij}^{(l)}$ .
17:                                     ▷ Reshape  $\mathbf{V}_{k,l}$  into spatial map  $\mathbf{SM}_{k,l} \in \mathbb{R}^{D \times D}$ 
18:     $\mathbf{SM}_{k,l} = \mathcal{M}_{\text{reshape}}(\mathbf{V}_{k,l})$ .
19:                                     ▷ Accumulate  $\mathbf{SM}_{k,l}$  into  $\mathbf{S}_k$ 
20:     $\mathbf{S}_k \leftarrow \mathbf{S}_k + \mathbf{SM}_{k,l}$                                      ▷ Element-wise addition
21:  end for
22: end for
23:
24: return  $\{\mathbf{S}_k \mid k = 1, \dots, K\}$ 

```

The first stage, detailed in Algorithm 1, computes attention-based similarity maps $\{\mathbf{S}_k\}_{k=1}^K$. For each reference image I_k , this algorithm probes the layers \mathcal{L} of the unified multimodal diffusion model U . It aggregates the attention from latent tokens $i \in \mathcal{D}_{\text{latent}}$ to the image tokens $j \in \mathcal{D}_{\text{img},k}$ corresponding to I_k . This aggregated attention is reshaped via $\mathcal{M}_{\text{reshape}}$ into a $D \times D$ spatial map $\mathbf{SM}_{k,l}$ for each layer l . These layer-specific maps are then accumulated to form the final similarity map $\mathbf{S}_k \in \mathbb{R}^{D \times D}$. Each \mathbf{S}_k thus highlights regions in the $D \times D$ latent space which exhibit strong attention probability with the k -th reference image.

The second stage, outlined in Algorithm 2, uses the similarity maps \mathbf{S}_k (generated by Algorithm 1) to derive the final binary segmentation maps $\mathcal{R}_k \in \{0, 1\}^{D \times D}$ which represent the ROIs. This algorithm takes as input the predicted latent at $t = 0$, $\hat{\mathbf{O}}_{\text{int},0}$ and outputs a set of K assigned binary segmentation maps $\{\mathcal{R}_k \in \{0, 1\}^{D \times D}\}_{k=1}^K$.

We first generate the estimated image from the predicted latent $\hat{\mathbf{O}}_{\text{int},0}$ by passing through the VAE Decoder D_{VAE} . This is then segmented using the Segment Anything 2 [31] model, denoted SAM , to produce initial segmentation masks $\{\mathbf{M}_{seg,j}\}$. These masks are subsequently refined by Non-Maximum Suppression (NMS) to yield Q binary segmentation maps $\{\mathbf{G}_q\}_{q=1}^Q$. These maps \mathbf{G}_q are transformed to $D \times D$ resolution required for comparison with the similarity maps \mathbf{S}_k , and represent the candidate regions within the decoded image. If no regions survive NMS ($Q = 0$), the algorithm initializes all output maps \mathcal{R}_k to one and terminates.

Algorithm 2 Assign Regions for each Reference Image

Inputs:

- Predicted latent at $t = 0$: $\hat{\mathbf{O}}_{\text{int},0} \in \mathbb{R}^{dim_{lat}}$.
- VAE Decoder D_{VAE} .
- Segmentation Model SAM .
- NMS threshold θ_{NMS} .
- Set of K similarity maps $\{\mathbf{S}_k \in \mathbb{R}^{D \times D}\}_{k=1}^K$ (from Alg. 1).
- Number of input reference images K .

Outputs:

- Set of K assigned generated segmentation maps $\{\mathcal{R}_k \in \{0, 1\}^{D \times D}\}_{k=1}^K$.
-

```

1:                                     ▷ Step 1: Generate Segmentation Maps from  $\hat{\mathbf{O}}_{\text{int},0}$ 
2:  $\{\mathbf{M}_{seg,j}\}_{j=1}^{Q'} \leftarrow SAM(D_{VAE}(\hat{\mathbf{O}}_{\text{int},0}))$ .                                     ▷ Segment VAE decoder output.
3:  $\{\mathbf{G}_q \in \{0, 1\}^{D \times D}\}_{q=1}^Q \leftarrow NMS(\{\mathbf{M}_{seg,j}\}_{j=1}^{Q'}, \theta_{NMS})$ .   ▷  $Q$  maps post-NMS, at  $D \times D$  res.
4:                                     ▷ Step 2: Construct Cost Matrix  $\mathbf{C} \in \mathbb{R}^{K \times Q}$ 
5: for  $k = 1, \dots, K$  do
6:   for  $q = 1, \dots, Q$  do
7:      $\mathbf{C}[k, q] = -\sum_{p=1}^D \sum_{r=1}^D (\mathbf{S}_k[p, r] \cdot \mathbf{G}_q[p, r])$ .           ▷ Negative overlap score.
8:   end for
9: end for
10:
11:                                     ▷ Step 3: Apply Hungarian Algorithm
12:  $\mathcal{A} \leftarrow Hungarian(\mathbf{C})$ .                                     ▷  $\mathcal{A}$  is set of optimal  $(k, q)$  pairs.
13:
14:                                     ▷ Step 4: Formulate Final Output  $\mathcal{R}_k$ 
15: Initialize  $\mathcal{R}_k$  as  $D \times D$  ones matrix for  $k = 1, \dots, K$ .
16: for each assignment  $(k^*, q^*) \in \mathcal{A}$  do
17:    $\mathcal{R}_{k^*} \leftarrow \mathbf{G}_{q^*}$ .
18: end for
19:
20: return  $\{\mathcal{R}_k\}_{k=1}^K$ .

```

If $Q > 0$, a $K \times Q$ cost matrix \mathbf{C} is constructed to evaluate the compatibility between each reference image I_k (via its similarity map \mathbf{S}_k) and each generated segmentation map \mathbf{G}_q . We compute the

cost of assigning generated region \mathbf{G}_q to reference image I_k , $\mathbf{C}[k, q]$, from the overlap between \mathbf{G}_q and the similarity map \mathbf{S}_k (Algorithm 2, Line 14). The Hungarian algorithm [21] is then applied to minimize the cost matrix \mathbf{C} . This yields a set \mathcal{A} of optimal assignment pairs (k, q) , where each reference image k is matched to at most one generated map q .

Finally, the output maps $\{\mathcal{R}_k\}$ are first initialized to $D \times D$ ones matrices. For each optimal assignment $(k^*, q^*) \in \mathcal{A}$, the corresponding generated segmentation map \mathbf{G}_{q^*} is assigned as the output map \mathcal{R}_{k^*} for the reference image I_{k^*} . If a reference image I_k is not part of any assignment in \mathcal{A} (e.g., if $K > Q$), its \mathcal{R}_k remains a ones map.

Once we find the region assignments $\{\mathcal{R}_k\}_{k=1}^K$, we apply the Unified Isolated Attention approach explained in Section 3 to generate the final image.

MH-IR-Diffusion: For models like IR-Diffusion that involve generating an initial image I_{gen} , followed by a final image with specific identities, we can determine regions \mathcal{R}_k by directly matching facial identity cues. This method uses ArcFace embeddings to associate faces segmented from I_{gen} with the K input reference images I_k . The segmentation mask of an assigned face in I_{gen} serves as the ROI \mathcal{R}_k .

We show our approach in Algorithm 3. Initially, *SAM* and NMS are used to obtain Q distinct face segmentation masks $\{\mathbf{G}_q\}$ from I_{gen} . ArcFace embeddings are then computed for these generated face regions $\{\mathbf{e}_{gen,q}\}$ and for the reference images $\{\mathbf{e}_{ref,k}\}$. A cost matrix \mathbf{C} is built using the cosine dissimilarity ($1 - \text{cosine_similarity}$) between these embeddings. The Hungarian algorithm then finds the optimal assignment \mathcal{A} between reference images and generated faces. For each match, the corresponding mask \mathbf{G}_{q^*} is designated as \mathcal{R}_{k^*} . These pixel-space masks \mathcal{R}_k are then available for subsequent processing steps.

D Baselines and Implementation Details

In this Section, we highlight our Implementation Details for our baselines. Every experiment was performed on an Nvidia Tesla A100 GPU.

OmniGen. We used the official implementation of OmniGen² and prompted it for multi-human with and without pose conditioning. We run the default settings of 50-step inference, with a text-guidance of 2.5. For Task-1, we set image guidance scale at 2.0, and for Task-2, we found the best results with 2.8. We implemented MH-OmniGen over this repository.

UniPortrait. We used the official implementation of UniPortrait³ and used all the default hyper-parameters. From the original settings, we perform a 25-step inference at a guidance scale of 7.5. For pose conditioning, UniPortrait adopts controlnet, for which we set the guidance scale at 1.

FastComposer. We used the official implementation of FastComposer⁴ and used all the default hyper-parameters. From the original settings, we perform a 50-step inference at a guidance scale of 5.

OMG. We used the official implementation of OMG⁵, and used the the InstantID version. As the performance was poor without ControlNet, we only report the performance with regional priors, and used all the default hyper-parameters. The inference is run in 50 steps, using a CFG scale of 3.0. The controlnet and InstantID models both were weighted at 0.8, as per original implementation. To make the performance suitable to MultiHuman, we modified their detection algorithm to match all detected humans (instead of the default matching with "man" and "woman").

Regional-PuLID. We used the official implementation of Regional-PuLID⁶ and made it compatible with Multi-human generation with default box priors based on number of humans. We found best results with base ratio set to 0.3. We kept the remaining hyperparameters at default settings. These include 24 inference steps and a guidance scale of 3.5.

²<https://github.com/VectorSpaceLab/OmniGen>

³<https://github.com/junjiehe96/UniPortrait/tree/main>

⁴<https://github.com/mit-han-lab/fastcomposer/tree/main>

⁵<https://github.com/kongzhecn/OMG.git>

⁶<https://github.com/instantX-research/Regional-Prompting-FLUX>

Algorithm 3 Assign Regions for MH-IR-Diffusion using ArcFace Embeddings

Inputs:

- Generated image I_{gen} ($H \times W$).
- Set of K generated reference images $\{I_k\}_{k=1}^K$.
- Segmentation Model SAM (for face segmentation).
- NMS threshold θ_{NMS} .
- ArcFace embedding function $ArcFace$.

Outputs:

- Set of K assigned face segmentation masks $\{\mathcal{R}_k \in \{0, 1\}^{H \times W}\}_{k=1}^K$.
-

```
1:                                     ▷ Step 1: Segment faces in  $I_{gen}$  and compute their ArcFace embeddings
2:  $\{\mathbf{M}_{seg,j}\}_{j=1}^{Q'} \leftarrow SAM(I_{gen})$ .
3:  $\{\mathbf{G}_q \in \{0, 1\}^{H \times W}\}_{q=1}^Q \leftarrow NMS(\{\mathbf{M}_{seg,j}\}_{j=1}^{Q'}, \theta_{NMS})$ .
4: for  $q = 1, \dots, Q$  do
5:    $\mathbf{e}_{gen,q} \leftarrow ArcFace(I_{gen}, \mathbf{G}_q)$ .                                     ▷ Embedding for face in  $I_{gen}$  at mask  $\mathbf{G}_q$ .
6: end for
7:
8:                                     ▷ Step 2: Compute ArcFace embeddings for  $I_k$ 
9: for  $k = 1, \dots, K$  do
10:   $\mathbf{e}_{ref,k} \leftarrow ArcFace(I_k)$ .
11: end for
12:
13:                                     ▷ Step 3: Construct Cost Matrix  $\mathbf{C} \in \mathbb{R}^{K \times Q}$ 
14: for  $k = 1, \dots, K$  do
15:   for  $q = 1, \dots, Q$  do
16:      $\mathbf{C}[k, q] = 1 - \text{cosine\_similarity}(\mathbf{e}_{ref,k}, \mathbf{e}_{gen,q})$ .
17:   end for
18: end for
19:
20:                                     ▷ Step 4: Apply Hungarian Algorithm
21:  $\mathcal{A} \leftarrow \text{Hungarian}(\mathbf{C})$ .
22:
23:                                     ▷ Step 5: Formulate Final Output  $\mathcal{R}_k$ 
24: Initialize  $\mathcal{R}_k$  as  $H \times W$  zeros matrix for  $k = 1, \dots, K$ .
25: for each assignment  $(k^*, q^*) \in \mathcal{A}$  do
26:    $\mathcal{R}_{k^*} \leftarrow \mathbf{G}_{q^*}$ .
27: end for
28:
29: return  $\{\mathcal{R}_k\}_{k=1}^K$ .
```

LoRA/MuDI. We used the official implementation of MuDI⁷ and trained a single LoRA for every sample. We used the default settings for training, with 2000 steps at a learning rate of $1e^{-4}$. We train in two settings, with a single view per face and 5 views per face. During inference, we kept the default setting with an inference of 50 steps and guidance scale of 5. We run inference with both LoRA and MuDI using the provided examples. For LoRA with pose, we use the SDXL openpose controlnet with a scale of 1.0.

MIP-Adapter. We used the official implementation of MIP-Adapter⁸, which builds upon a pretrained IP-Adapter and SDXL model, and incorporates OpenCLIP-ViT-bigG/14 as the image encoder. We loaded the released MIP-Adapter weights into this framework to better support multi-subject generation. For multi-human generation, we used prompts from our MultiHuman-Testbench and

⁷<https://github.com/agwmon/MuDI>

⁸<https://github.com/hqhQAQ/MIP-Adapter>

adopted the DDIM sampler with 30 inference steps and a guidance scale of 7.5. The IP-Adapter scale was set to 0.75. For pose-based regional conditioning, we followed the ControlNet implementation⁹.

IP-Adapter. While the pretrained IP-Adapter provides strong performance, it is not designed to directly support multiple reference images. To address this, we adopted the MIP-Adapter framework to leverage its mechanism of weight merging within the adapter layers, without loading the MIP-Adapter weights. Instead, we retained only the pretrained IP-Adapter weights in our implementation. Sampling parameters, including 30 inference steps, guidance scale of 7.5, and IP-Adapter scale of 0.75, were set identically to those in MIP-Adapter for consistency.

RectifID. We utilize the official implementation provided by the authors¹⁰. Following their setup, we adopt a modified version of Stable Diffusion 1.5 released by Perflow¹¹, which is pretrained on the LAION-Aesthetic-5+ dataset with a particular focus on human faces and subject-centric generation. For the inversion process, we perform 50 sampling steps using classifier-free guidance with a guidance scale of 3.0. In experiments involving ControlNet, all settings are kept identical except for the use of ControlNet weights¹².

λ -Eclipse. We employed the official implementation provided by the authors¹³, a model designed for multi-concept personalized text-to-image generation. This model operates within the CLIP latent space and is specifically tailored to work with the Kandinsky v2.2 [34] diffusion image generator. For inference, we employed the DDIM sampler with 50 steps and a guidance scale of 7.5. All experiments were conducted using the provided scripts and configurations to ensure consistency and reproducibility.

E Additional Quantitative Results

In this Section, we provide additional Quantitative analysis on the MultiHuman Testbench, as an extension to Section 5 of the paper. The main results from Section 5 are summarized in the Radar graphs in Figure E.1.

E.1 Performance across varying number of people

In this Section, we study Multi-ID similarity scores and Person Count for methods performing Task 1, across different number of people. This is an extension to Table 3 in the main paper.

Summarized in Table E.1, we consistently observe that the ability to maintain ID Similarity deteriorates across all models as the number of faces in the generated image increases from two to five. This indicates a general bias where identity preservation becomes significantly more challenging with growing scene complexity. However, the magnitude and nature of this drop vary between methods. Methods such as UniPortrait, OmniGen, and MH-OmniGen start with relatively high ID Similarity scores for one or two people, indicating strong initial performance. As the person count increases, they experience substantial absolute drops in ID Similarity. For instance, MH-OmniGen’s score falls from 65.3 at two people to 38.0 at five people. Fastcomposer begins with a significantly lower ID Similarity even for just two people (15.3) and suffers the most dramatic percentage drop, falling to 5.9 at five people. GPT-Image-1 starts at a moderate ID Similarity score for two people (31.8) and exhibits the least severe relative decrease in performance as the person count increases, resulting in a score of 24.9 at five people. From the Person Count results, it is clear that GPT-Image-1 is more accurate in generating images with the correct number of people, compared to other methods, which fail often for more than three people.

E.2 Measuring Bias in Multi-Human Generation

Using the labeled attributes provided with the data, we provide a study on the biases for each method in Task 1 and Task 2. We measure the single-person ID similarity and report it across various splits: Ethnicity(E.2), age, gender and status(E.3). Based on the ID-Similarity scores highlighted in red in

⁹<https://huggingface.co/thibaud/controlnet-openpose-sdxl-1.0>

¹⁰<https://github.com/feifeiobama/RectifID>

¹¹<https://huggingface.co/hansyan/perflow-sd15-dreamshaper>

¹²https://huggingface.co/llyasviel/control_v11p_sd15_openpose

¹³<https://github.com/eclipse-t2i/lambda-eclipse-inference>

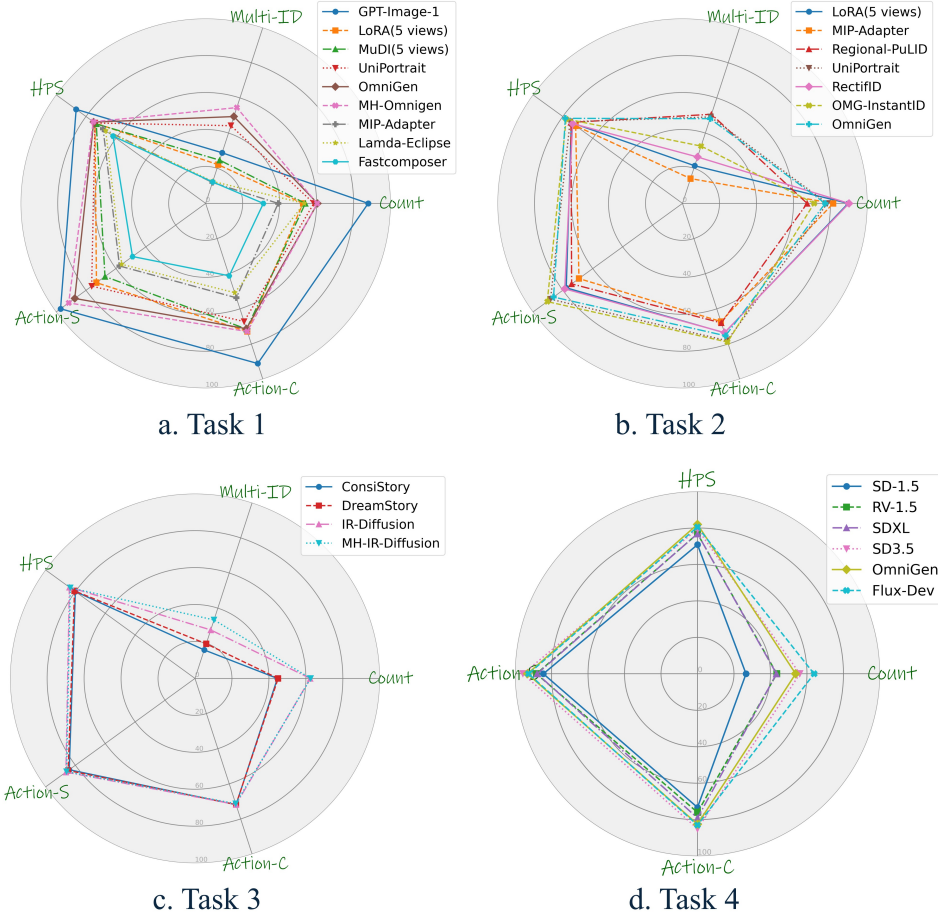


Figure E.1: **Radar Graphs.** Visualizing performance on Tasks 1,2,3,4 using Radar Graphs.

Model	Multi-ID Similarity					Person Count				
	2	3	4	5	Avg(1-5)	2	3	4	5	Avg(1-5)
Task 1: Reference-based Multi-Human Generation in the Wild										
GPT-Image-1	31.8	29.5	27.8	24.9	28.8	90.7	91.8	89.5	75.3	87.9
Fastcomposer	15.3	7.4	7.2	5.9	12.2	62.9	11.2	3.2	1.1	31.2
Uniportrait	56.5	46.4	33.8	28.6	44.2	90.6	76.3	23.7	14.1	58.5
OmniGen	60.8	52.3	42.2	35.2	49.4	88.8	88.0	23.2	21.6	60.5
MH-OmniGen	65.3	60.4	45.1	38.0	54.5	91.2	87.5	22.4	19.7	60.3

Table E.1: Studying the ID similarity and Person count metrics for different number of people, for Multi-Human Generation in the Wild.

Table E.2 and Table E.3, biases are evident in how different models and their backbones perform. These biases are indicated by deviations from the average score for each row. A darker red shades signifies higher bias.

In Task 1, GPT-Image-1 (GPT-4o) shows a positive bias for South-Asian identities and a positive bias for Aged individuals. UniPortrait (RV1.5) exhibits positive biases favoring White and East-Asian faces while underperforming on Black individuals. Additionally, it heavily underperforms on Aged individuals by demographic type, offset by a positive bias for Young Adults. Fastcomposer (SD1.5) shows minimal racial/ethnic bias but has a light negative bias for Celeb faces. OmniGen (Phi-3) and MH-OmniGen (Phi-3) generally display less pronounced biases in Task 1, showing mostly light biases favoring White and South-Asian faces by race/ethnicity, suggesting more balanced performance compared to the rest.

Model	Backbone	ID-Similarity					
		White	Black	South-Asian	East-Asian	Hispanic	Middle-East
Task 1: Reference-based Multi-Human Generation in the Wild							
GPT-Image-1	GPT-4o	26.4	28.8	30.2	26.2	27.5	28.2
UniPortrait	RV1.5	41.1	36.8	38.3	41.8	37.5	38.4
Fastcomposer	SD1.5	8.7	8.8	9.3	9.5	9.2	8.9
OmniGen	Phi-3	44.0	45.1	47.0	45.0	45.5	44.3
MH-OmniGen	Phi-3	48.4	49.3	51.6	50.0	49.7	49.0
Task 2: Reference-based Multi-Human Generation with Regional Priors							
UniPortrait	RV1.5	48.9	43.6	45.3	47.3	43.3	45.3
RectifID	SD1.5	17.6	16.9	19.2	21.1	16.3	17.1
Regional-PuLID	Flux	47.4	44.1	47.9	52.6	47.3	46.0
OMG-InstantID	SDXL	26.8	24.3	27.0	30.6	25.9	25.1
OmniGen	Phi-3	42.7	42.6	44.9	43.6	41.4	41.2

Table E.2: Multi-Human Generation with Reference Images: Multi-Human Tuning-Free Models with ID-Similarity Metrics by Race/Ethnicity (Backbone Removed)

Turning to Task 2, where regional priors are used, the patterns of bias shift for some models. UniPortrait (RV1.5) continues to show biases favoring White and East-Asian faces and against Black and Hispanic faces, favoring female faces to male faces, and heavily favoring young adults. RectifID (SD1.5) shows a bias favoring East-Asian faces by race/ethnicity. Regional-PuLID (Flux) displays significant biases, with a strong positive bias for East-Asian individuals and a negative bias against Black faces by ethnicity. By demographic, Regional-PuLID exhibits strong biases against Males and Aged faces, while strongly favoring Female, Young Adult, and Celeb identities. OMG-InstantID (SDXL) shows a bias against Black faces and favoring East-Asian faces, and favors Young Adults. OmniGen (Phi-3) in Task 2 shows less prominent biases, with a bias favoring South-Asian faces and light biases against Hispanic and Middle-East faces by ethnicity.

Model	Backbone	ID-Similarity						
		Male	Female	Young Adult	Middle Aged	Aged	Celeb	Anonymous
Task 1: Reference-based Multi-Human Generation in the Wild								
GPT-Image-1	GPT-4o	29.8	26.0	26.0	28.8	30.8	28.1	26.6
UniPortrait	RV1.5	37.5	40.5	40.7	37.7	30.7	37.6	39.3
Fastcomposer	SD1.5	9.0	9.1	9.2	9.1	8.5	7.1	9.5
OmniGen	Phi-3	44.9	45.4	44.3	46.0	45.4	45.5	43.7
MH-OmniGen	Phi-3	49.5	49.8	49.0	49.9	50.7	48.7	49.9
Task 2: Reference-based Multi-Human Generation with Regional Priors								
UniPortrait	RV1.5	43.5	47.7	48.2	44.0	42.9	46.9	45.3
RectifID	SD1.5	17.4	18.6	19.1	17.4	16.1	19.5	17.7
Regional-PuLID	Flux	42.3	52.5	51.7	45.4	41.5	50.5	46.9
OMG-InstantID	SDXL	25.0	28.2	28.7	25.1	24.9	24.9	26.8
OmniGen	Phi-3	43.6	42.1	41.8	43.2	44.6	42.6	42.9

Table E.3: Multi-Human Generation with Reference Images: Multi-Human Tuning-Free Models with ID-Similarity Metrics by Demographic and Type (Backbone Removed)

E.3 Effect of Our Pose Priors

Table E.4 shows the effect of adding our human-rectified regional pose priors. As observed, all metrics significantly improve in case of most methods. There is a slight drop in Multi-ID and Action-S for OmniGen, and a slight drop in Multi-ID in LoRA. Overall, regional pose priors can help generate significantly better results, as they make the task easier. However, this benefit comes with a severe hit to usability, which is why solving Task 1 is important.

F Additional Qualitative Results

In this Section, we provide additional Qualitative results to supplement the ones in Section 5 of the main text.

Model	Count		Multi-ID		HPS		Action-S		Action-C	
	Task 1	Task 2	Task 1	Task 2	Task 1	Task 2	Task 1	Task 2	Task 1	Task 2
LoRA(5 views)	52.6	89.6	22.0	21.4	25.9	26.0	73.0	77.7	72.9	73.6
MIP-Adapter	39.2	81.5	11.9	14.1	24.0	25.0	57.6	69.2	53.7	67.2
UniPortrait	58.5	78.3	44.2	49.2	25.9	26.3	76.2	88.2	67.2	78.1
RectifID	37.8	90.1	18.6	26.4	24.8	25.7	67.3	78.7	68.2	73.5
OmniGen	60.5	77.2	49.4	48.2	26.2	27.4	87.5	86.2	71.3	75.3

Table E.4: Comparison of Multi-Human Generation Metrics With and Without Regional Priors for Tuning-Free Models

F.1 Improvements from MH-OmniGen

Figure F.1 shows more qualitative results on Multi-Human generation in the wild, using OmniGen and MH-OmniGen. As observed, MH-OmniGen is able to correct many instances of subject blending using our proposed Unified Region Isolation and Implicit Matching algorithm.

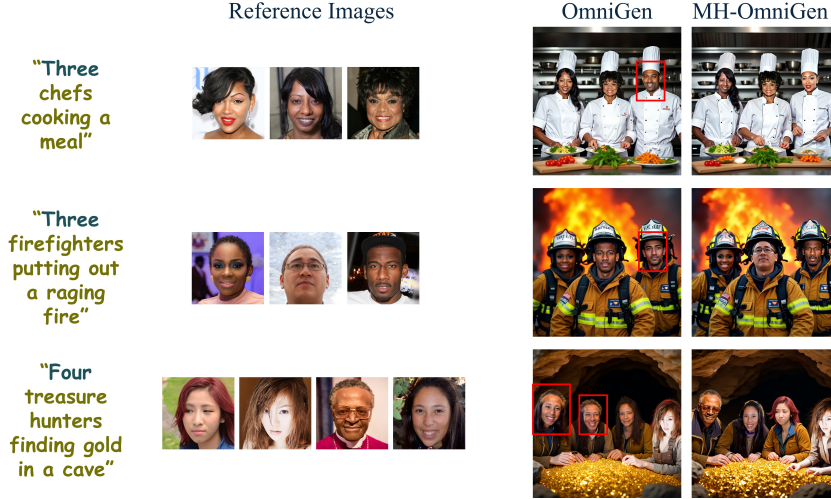


Figure F.1: **Qualitative Results for MH-OmniGen v/s OmniGen on Task 1.** As observed, MH-OmniGen is able to significantly improve OmniGen by reducing ID leakage, which is highlighted with red boxes.

F.2 Qualitative results for Task 2: Regional Priors

Figure F.2 shows the best performing methods: RectifID, UniPortrait, LoRA, OmniGen and Regional-PuLID(with box priors) on Task 2: Reference-based Multi-Human Generation with Regional Priors. As observed in the figure, OmniGen, UniPortrait and Regional-PuLID show best results. However, it is clear that each method has severe limitations including incorrect count accuracy and underperformance on ID similarity. This underlines a huge scope for improvement.

F.3 Qualitative results for Task 4: Text-to-Image generation

Figure F.3 shows the best performing methods on Task 4: Text-to-Image Generation for Multiple Humans (with no reference images). The methods on display are RV1.5, SDXL, SD3.5, OmniGen and Flux. Flux and OmniGen show best results. However, it is clear that all methods show limitations in terms of count accuracy. Additionally, every method is susceptible to generating faces of people with similar attributes (age, race, gender). We believe that there is a heavy scope for improvement for Generation Models in this regard.

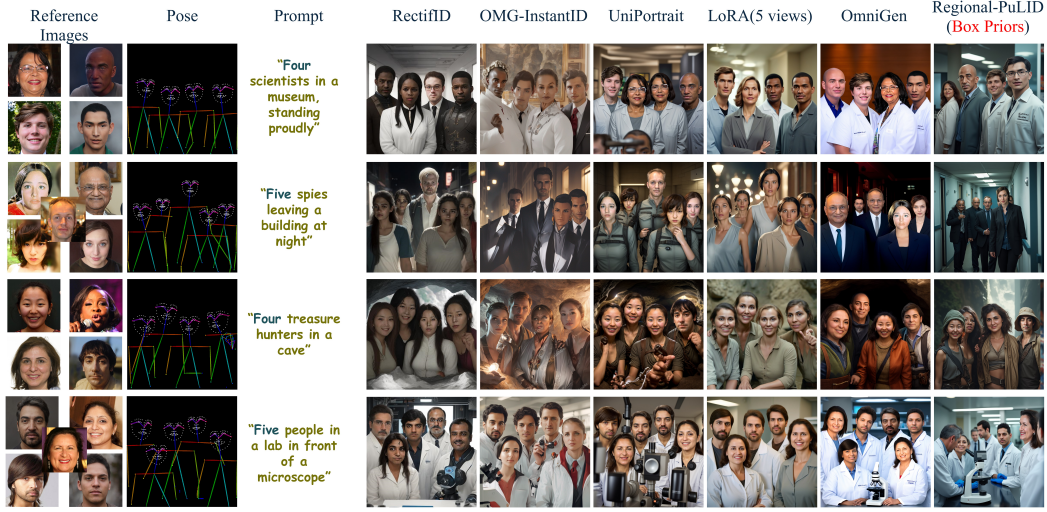


Figure F.2: **Qualitative Results on Multi-Human Generation with Pose conditioning.** The image shows the best performing methods: RectifID, UniPortrait, LoRA, OmniGen and Regional-PuLID(with box priors). OmniGen, UniPortrait and Regional-PuLID show best results albeit with severe limitations.

G Societal Impact

With MultiHuman-Testbench, we aim to make significant advancements in AI-driven multi-human image generation, and we anticipate substantial positive societal benefits. By encouraging the development of models which accurately depict diverse individuals across age, ethnicity, and gender while preserving their identities in complex scenes, we hope to contribute to more equitable and inclusive digital media. We envision that our benchmark can enhance creative tools for artists and developers, enrich AR/VR/XR experiences, and improve assistive technologies. Furthermore, we believe that our proposed standardized evaluation suite will accelerate research and offer clearer insights into generation model capabilities.

However, we also recognize that this progress amplifies societal risks. The capability for highly realistic multi-human image generation increases the potential for deepfakes which could be used in misinformation campaigns or impersonation, thereby posing threats to individual privacy and societal trust. Finally, we acknowledge that the increasing sophistication of these generative tools raises concerns about job displacement in creative sectors. Hence, we request the broader community to proactively engage in developing ethical frameworks, and responsible use guidelines.



Figure F.3: **Qualitative Results on Multi-Human Generation for Text-to-Image models.** The image shows the best performing methods on Task 4: RV1.5, SDXL, SD3.5, OmniGen and Flux. Flux and OmniGen show best results albeit all methods show limitations in terms of count accuracy.